Stability and Electronic Characteristics of Epitaxial Silicene Multilayers on Ag(111)

Neil W. Johnson, David Muir, Ernst Z. Kurmaev, and Alexander Moewes*

In this study, the stability and electronic characteristics of epitaxial silicene bilayers and multilayers on the Ag(111) surface are investigated through synchrotron-based soft X-ray emission and absorption spectroscopy and first-principles, full-potential density functional theory simulations. The calculations predict a novel tristable AA-stacked bilayer structure that can explain the ($\sqrt{3} \times \sqrt{3}$)R30° honeycomb topography commonly observed through scanning tunneling microscopy and noncontact atomic force microscopy. It is reported that the electronic structure of this epitaxial bilayer is similar to those of epitaxial monolayers on Ag(111), namely, metallic and showing significant interaction with the underlying substrate. However, the soft X-ray spectroscopy experiments suggest that during multilayer growth a majority of the epitaxial silicon reverts to a bulk-like state, a result that has significant implications toward the existence of large-area epitaxial silicene multilayers.

1. Introduction

2D electronic materials such as graphene and its silicon-based analogue silicene have been the focus of intense research of late due to their unique set of electronic, magnetic, thermal, and mechanical properties.[1,2] As freestanding sheets of silicene are yet to be observed, research into this promising new material has generally fallen into one of two camps: theoretical simulations of freestanding silicene with a variety of external conditions and chemical modifications, and the experimental characterization of epitaxial 2D silicon sheets deposited on various substrates.

Theoretically, freestanding silicene is expected to possess a Dirac cone electronic structure similar to that of graphene,[3,4] albeit with a small but finite bandgap opening due to the effects of spin-orbit coupling.[5] This suggests that if stable freestanding silicene were to be realized, it should be a candidate for many of the same applications for which graphene is currently being considered. In fact, silicene may even have some advantages over its carbon-based counterpart. Its inherent buckling could allow for bandgap control,[6] spin polarization control,[7] and an ambipolar field effect[3] all through the application of a gating voltage on an undoped freestanding silicene sheet. In addition, the transition to 2D electronics design and manufacturing should be much smoother if it remains based around the same element (silicon) as current 3D processes.

On the experimental side, honeycomb monolayer (ML) lattices of Si atoms have been observed on the Ag(111) face,[8–13] the Ir(111) face,[14] MoS_2,[15] and the ZrB_2 (0001) face.[16] Further, stable MLs have been theoretically predicted on SiC(0001)[17] and h-BN.[17,18] However, the degree to which these epitaxial MLs actually represent freestanding silicene has been called into question. The most thoroughly studied epitaxial silicene samples are those deposited on Ag(111), which were first observed in 2012 when Vogt et al.[8] reported a (3×3) silicene supercell commensurate with the (4×4) Ag(111) supercell (hereafter referred to as the (3×3)/(4×4) ML). Since then, a number of rotated ($\sqrt{7} \times \sqrt{7}$)R19.1° silicene MLs have been identified on the ($\sqrt{13} \times \sqrt{13}$)R13.9° Ag(111) supercell[9–12,19] (hereafter the ($\sqrt{7} \times \sqrt{7}$)/($\sqrt{13} \times \sqrt{13}$) ML), and an unstable and highly defective ($\sqrt{7} \times \sqrt{7}$) silicene reconstruction on the ($2\sqrt{3} \times 2\sqrt{3}$)R30° Ag(111) cell.[20] Initially, it was thought that the prototypical (3×3)/(4×4) ML bore the hallmarks of a Dirac cone in its electronic structure.[8] However, it has now been shown that these ML configurations result in a metallic Si sheet interacting significantly with the underlying Ag substrate. As such, the resulting electronic structure is not desirable for 2D electronic applications. This result has now been reproduced through a number of theoretical and experimental techniques, including density functional theory (DFT) calculations,[13,21–23] angle-resolved photoemission spectroscopy (ARPES),[22] scanning tunneling spectroscopy[24] (STS), and soft X-ray emission and absorption spectroscopies[13] (XES and XAS, respectively). Epitaxial silicene ML research now primarily focuses on functionalization of the ML in order to weaken its interaction with the Ag(111), or ML silicene deposition on alternative, typically nonmetallic substrates.

Recently, a major development in silicene research occurred when the first silicene-based transistor was manufactured and

N. W. Johnson, Prof. A. Moewes
Department of Physics and Engineering Physics
University of Saskatchewan
116 Science Place, Saskatoon S7N 5E2, Canada
E-mail: johnson.neil@usask.ca
Dr. D. Muir
Canadian Light Source, 44 Innovation Boulevard
Saskatoon S7N 2V3, Canada
Dr. E. Z. Kurmaev
M. N. Mikheev Institute of Metal Physics
Ural Branch of the Russian Academy of Sciences
620990, Yekaterinburg GSP-170, Russia
Dr. E. Z. Kurmaev
Technological Institute
Ural Federal University
Mira Street 19, 620002 Yekaterinburg, Russia

DOI: 10.1002/adfm.201501029

characterized, representing the first time epitaxial silicene has been observed away from its growth substrate.[25] Though the charge carrier mobility in the device was much lower than the theoretically predicted values for freestanding silicene and the monolayer rapidly oxidized after exposure, this achievement serves as an important step toward realizing silicene-based technology. Passivation from atmospheric oxygen and the influence of the growth and transistor substrates will be essential to improving the performance and stability of silicene-based devices. Production of a silicene multilayer could serve both of these purposes simultaneously, and it has even been suggested that a multilayer of silicene grown on the Ag(111) surface might be host to a Dirac cone electronic structure.[26,27]

Scanning tunneling microscopy[19,28,29] (STM) and low-energy electron diffraction[26,30] (LEED) patterns from depositions several times longer than what is required to create a ML indicate the formation of a structure with a $(\sqrt{3} \times \sqrt{3})$R30° periodicity relative to the (1×1) silicene ML unit cell, reportedly reconstructing through the deposition of enough Si to form tens of additional layers.[31] These structures are most often reported as having a hexagonal honeycomb appearance in STM, though the chemical nature of the tip apex can cause them to appear inverted in contrast, instead resembling a triangular lattice of large, bright points.[19] It has been suggested that the observed $(\sqrt{3} \times \sqrt{3})$R30° pattern could be a result of so-called "dumbbell" Si sites in an otherwise flat Si sheet, which is a highly stable configuration for isolated monolayers.[32,33] However, it is uncertain whether such a structure will exist on the Ag(111) substrate or can stack to form a multilayer.

Presently, there are two favored interpretations of the observed $(\sqrt{3} \times \sqrt{3})$R30° periodic structure: multilayer epitaxial silicene and bulk-like layers of Si(111) with an Ag-terminated surface. Bilayer (BL) silicene has been previously predicted to assume an AB-stacked configuration with a triangular lattice of protruding Si atoms in the upper layer.[34] This structure is tristable with a small energy barrier between each of the three inequivalent structures, and the superposition of the three will result in the appearance of a honeycomb lattice when viewed through STM. X-ray diffraction (XRD), Raman spectroscopy, and energy-dispersive X-ray reflectivity (EDXR) have all supported the conclusion that multilayer silicene is a distinct entity from Si(111).[31] In addition, the ARPES-derived band dispersion is not consistent with Ag-terminated Si(111).[30]

However, the epitaxial silicene model fails to adequately explain the LEED intensity–voltage (I/V) curves for samples with greater than 1 ML of Si deposition.[30] Instead, it has been suggested that both the LEED I/V curves and the honeycomb topography[29] correspond to the honeycomb-chained-triangle (HCT) or inequivalent triangle (IET) configurations of $(\sqrt{3} \times \sqrt{3})$R30° Ag on the Si(111) face. It is possible that both growth mechanisms can occur simultaneously, and that the presence or lack of Ag-segregation is highly sensitive to growth parameters such as substrate temperature or Si flux. Recent low-energy electron microscopy (LEEM) studies[35,36] determined that shortly after the completion of a ML, additional deposition results in the dewetting of the Si and the formation of bulk Si crystals. At present, it is not fully understood how the deposition of additional Si onto an epitaxial silicene ML will affect the electronic or atomic structure of the material.

In this study, we use full-potential all-electron DFT calculations to explore the atomic structures of silicene BLs on the Ag(111) face and compare them to experimental STM results. We identify a novel, tristable AA-stacked BL structure on the (4×4) Ag(111) unit cell that is more energetically favorable than the current AB-stacked model,[34] though the two look nearly identical in terms of topography. We also calculate their theoretical electronic structures to compare to the results of synchrotron-based XES and XAS performed on multilayer silicene samples at the Si $L_{2,3}$-edge. However, these measurements indicate that large-area multilayers do not form, as a significant proportion of the Si dewets into bulk-like Si crystals on the surface.

2. DFT Structural Relaxations of Epitaxial Bilayers

In order to calculate the electronic structure of BL epitaxial silicene, we must first determine a proper atomic structural model. In a typical silicene ML preparation the sample will consist of a mixture of $(3 \times 3)/(4 \times 4)$ and $(\sqrt{7} \times \sqrt{7})/(\sqrt{13} \times \sqrt{13})$ domains.[19] With a specific substrate temperature and deposition rate a nearly pure phase $(3 \times 3)/(4 \times 4)$ deposition can be achieved,[9] but the electronic characteristics of such a ML should be largely identical to the mixed-component ML.[13] The composition of any particular ML sample can be verified with LEED using an incident electron energy around 50 eV. With the deposition parameters used in our experiment, the LEED patterns show clearly that both types of silicene domain are present when a complete ML is formed (**Figure 1**a). Any BL that we are likely to achieve, then, could be commensurate with either the (4×4) or $(\sqrt{13} \times \sqrt{13})$ Ag(111) supercell and would initially have the (3×3) or one of the stable $(\sqrt{7} \times \sqrt{7})$ ML structures at its base. However, the addition of a second layer of Si atoms and the thermal energy available from the substrate (typically held at about 500 K during deposition) might cause a significant rearrangement of the initial ML, so it cannot be taken for granted that the underlying ML structures persist through the deposition of the BL.

In a previous study,[13] we evaluated several structural models of epitaxial MLs by simulating them as sheets of Si on either (111) face of a layer thick slab of Ag atoms. We based our initial Si atomic positions on existing STM data. STM topographies of epitaxial BLs do not provide us with a full picture of the BL structure, only a rough idea of the upper layer configuration. Therefore we must consider a larger number of initial configurations to obtain solutions that not only minimize internal forces on the atoms but also minimize the total energy of the unit cell in order to determine which solution is the most energetically likely to form. While we always initialize the topmost layer of Si atoms as a flat sheet in order to not force our final result to conform to the STM data, we consider cases in which the bottom layer of Si is initialized as a flat sheet, with simple buckling or with the lowest-energy ML silicene configuration belonging to each substrate supercell. We also consider both AA- and AB-stacked BLs, resulting in twelve total initial structures, six belonging to each of the (4×4) and $(\sqrt{13} \times \sqrt{13})$ Ag(111) substrate supercells. Structural relaxations are performed with the ab initio, full-potential LAPW+lo WIEN2k code.[37] The exchange-correlation energy is given by

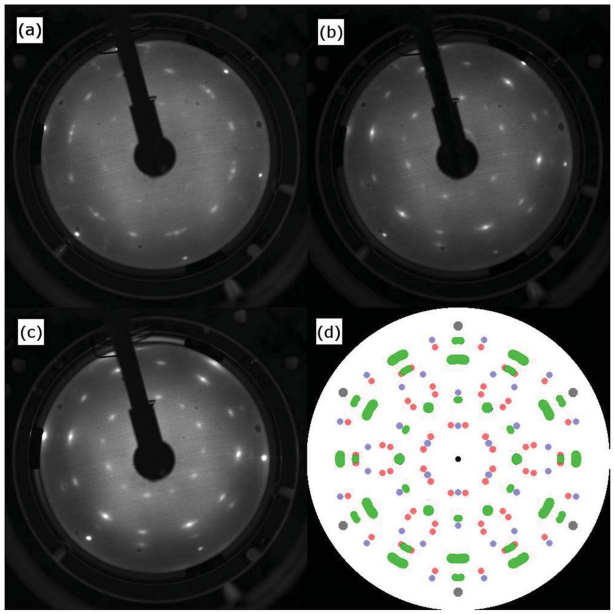

Figure 1. The LEED patterns after a) 1 h of Si deposition, b) 2 h, and c) 3 h. A mixed $(3 \times 3)/(4 \times 4)$ and $(\sqrt{7} \times \sqrt{7})/(\sqrt{13} \times \sqrt{13})$ ML will exhibit the LEED components shown in red and blue in (d), respectively, while a multilayer will increasingly show the features labeled with green in (d).

the generalized gradient approximation of Perdew, Burke, and Ernzerhof[38] (PBE-GGA) with a plane-wave cutoff of –6.0 Ry. After each iterative calculation cycle, the charge density in the system is updated and the resulting force on each atom is calculated. The internal atomic positions are then changed to reduce this force and the calculation cycle begins again. Convergence is reached when the forces in the system fall below 1 mRy au^{-1} on each mobile atom (the Ag atoms in the middle layer are fixed in position) and the total energy and charge steps in the self-consistent field cycle fall below 10^{-4} Ry and 10^{-3} e, respectively. To improve calculation efficiency the structural relaxations are performed on a $(3 \times 3 \times 1)$ k-point mesh with an RK_{max} of 5. When these parameters are later increased for the higher-accuracy electronic structure calculations, it is ensured that the forces on each atom still fall within acceptable levels.

We will begin our discussion with the structural optimization of AA- and AB-stacked freestanding silicene BLs in the absence of a supporting Ag(111) substrate. A previous calculation of the structural characteristics of freestanding silicene BLs[39] reported stability in the AA-stacked BL, but our full-potential calculations show that the AA-stacked system is unstable with a strong translational force between sheets that eventually settles it into an AB-stacking scheme. As a result, both the AA- and AB-stacked initial configurations converge to the same final freestanding structure, shown in **Figure 2**a,d. As would be expected of an sp^2/sp^3-hybridized system like silicene, the initially flat BLs become corrugated with a buckling of 0.68 Å, which is larger than the 0.44 Å buckling expected of freestanding, low-buckled ML silicene[3] and in agreement with the BL structure reported by Mohan et al.[39] Within each sheet, the average Si–Si distance is found to be 2.32 Å and the gap between the sheets is 2.53 Å, in good agreement with previously reported values. The vertically overlapping Si positions are shifted toward the centre of the BL, resulting in a bonding environment for these atoms that closely resembles that of a tetrahedral sp^3 network, aside from an elongated bond extending into the adjacent sheet.

Of the six epitaxial BL structures tested on the (4×4) Ag(111) supercell, all were found to eventually converge with a simple buckling scheme in their bottom layer. The lowest energy configuration, the AA-buckled structure shown in Figure 2b,e, was found to be about 0.15 eV per Si atom more stable than the next lowest energy structure, an AB-stacked structure that bears a striking resemblance to it apart from the stacking scheme. This slightly less energetically favorable structure was the subject of a previous DFT study[34] and will be discussed later. In our AA-stacked structure's bottom layer, the Si atoms are arranged in a simply buckled sheet with a 0.75 Å buckling height. The Si–Si distances range from 2.35 to 2.39 Å, and the bond angles within the hexagonal rings comprising the bottom layer are found to vary between 104.7° and 112.4°. All of the raised sites within the bottom layer have a lowered counterpart in the upper layer, with distances ranging from 2.45 to 2.48 Å between them. Notably, only 3 of the Si atoms residing above lowered sites in the bottom layer have emerged significantly from the upper layer's plane (about 1.2 Å above the lowest upper layer Si atom), with the rest only slightly buckled upward. As for the $(\sqrt{7} \times \sqrt{7})/(\sqrt{13} \times \sqrt{13})$ epitaxial BLs, four of the six structures were found to converge with a simple buckling scheme in the lower layer. The two that did not had about 0.5 eV per Si atom more total energy in the unit cell than the lowest energy configuration shown in Figure 2c,f, an AB-stacked BL. The simply buckled bottom layer has a buckling distance of about 0.81 Å with a Si–Si distance ranging between 2.38 and 2.42 Å and bond angles ranging from 108.3° to 111.9°. In this BL the upper layer is also essentially simply buckled with a structure that closely resembles a freestanding AB-stacked BL or a single plane of Si(111).

Once these atomic structures have been finalized, their electronic structures can be calculated. As mentioned earlier, these calculations take place on a denser k-point mesh of $(7 \times 7 \times 1)$ with an increased RK_{max} (5.5). We find that the calculated electronic structures are stable under further increasing these values to $(10 \times 10 \times 1)$ and 6.0, implying that our calculations are fully converged. However, before we delve into the electronic structure of these materials we will first complete the structural picture with a discussion of the spatial electron densities calculated on this denser mesh.

For an STM operating on a metallic surface in filled-states constant-height mode and with a small tip bias, the resulting STM signal will be approximately proportional to the total electron density between the tip bias energy and the Fermi level (E_F) at a certain point in space.[40] From our WIEN2k calculations, we are able to extract the total electron density between $E_F - 2$ eV and E_F in a plane 1.5 Å above the topmost Si atom for each of the bilayers shown in Figure 2. This results in the electron density plots shown in Figure 2g–i, which should bear resemblance to STM images of these freestanding and epitaxial BLs.

The simple buckling of the AB-stacked freestanding silicene BL produces a triangular lattice of points in the simulated STM with 3.85 Å between adjacent maxima. This topography does not conform to any known observation of the Si/Ag(111) surface, implying that BL silicene on Ag(111) cannot be considered to be freestanding. In the epitaxial BL commensurate with

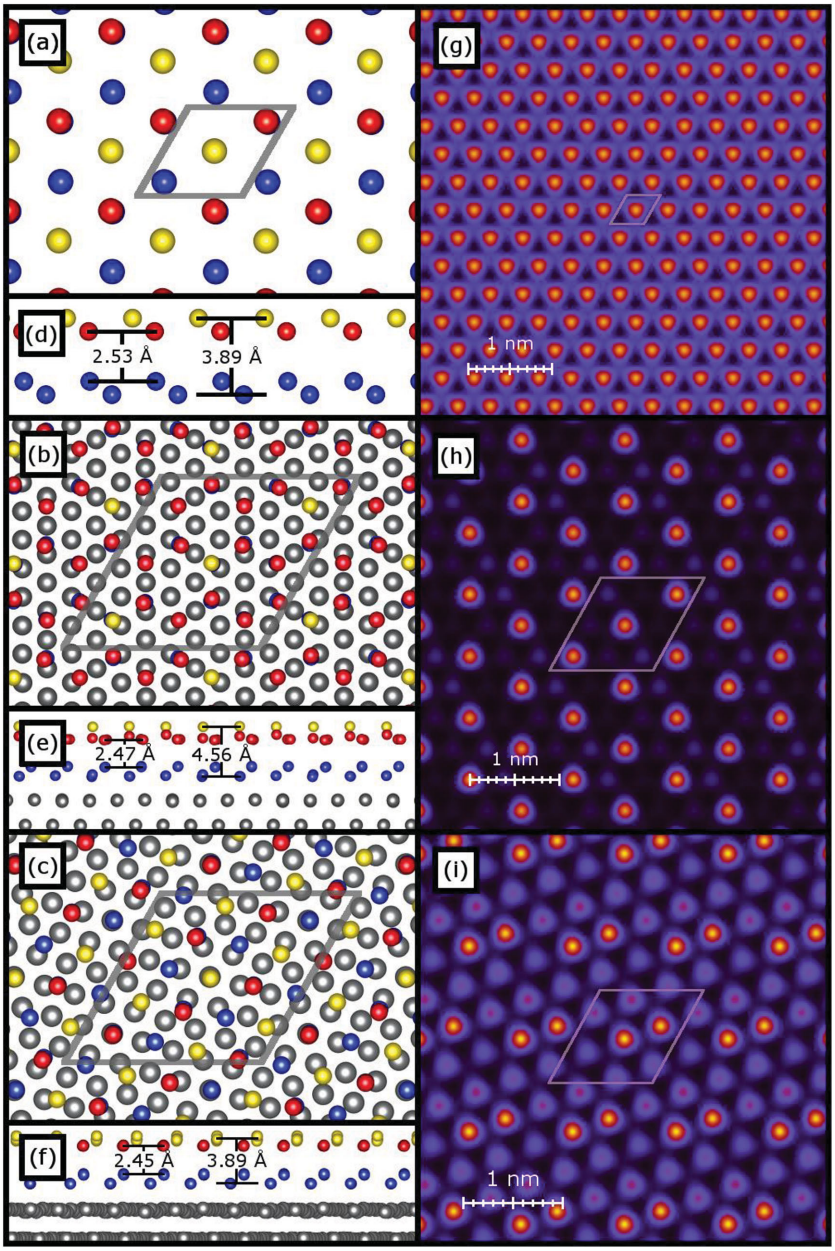

Figure 2. Top-down views of the freestanding $(3 \times 3)/(4 \times 4)$ and $(\sqrt{7} \times \sqrt{7})/(\sqrt{13} \times \sqrt{13})$ BLs are shown in (a–c), respectively. The unit cell boundaries of each are labeled with gray lines, centered on the most vertically prominent Si atom. Side views of the BLs are shown in (d–f), with distances between the various levels of the BL labeled. Charge density plots, which should resemble constant-height, filled-states, low bias STM images of the surfaces are shown in (g–i) on an arbitrary scale. Structural visualizations are provided by the VESTA software.[43]

the (4×4) Ag(111) substrate, the three vertically displaced Si atoms in the upper layer dominate the simulated STM pattern. This also results in a triangular lattice pattern, this time with a spacing of 6.65 Å. Finally, on the $(\sqrt{13} \times \sqrt{13})$ Ag(111) template, the simulated STM image consists of two triangular lattices: one is a result of the simple buckling and has a spacing of 3.95 Å and the other is the result of two top-layer Si sites that are raised slightly more than the others and has a periodicity equal to the unit cell dimension of 10.4 Å. As is the case with the freestanding BL, this topography does not conform to any known STM observations.

The novel AA-stacked BL on (4×4) Ag(111) is found to two have stable, energetically similar counterparts wherein the raised Si atoms are shifted by one honeycomb lattice position. This tristability, like that observed previously for the AB-stacked BL on (4×4) Ag(111),[34] allows for the reconciliation of the triangular lattice pattern shown in Figure 2h and the honeycomb pattern typically observed in STM measurements.[19,28,29] As we find that the AA-stacked BL configuration is energetically favored over the AB-stacked structure and that it is equally capable of explaining the existing STM data, we suggest that this novel structure is the most likely description of epitaxial BL silicene.

The lack of an observed STM topography that agrees with that predicted for the $(\sqrt{13} \times \sqrt{13})$ BL suggests that such a structure does not exist in multilayer silicene samples. It is feasible that, due to this reduced substrate interaction, $(\sqrt{7} \times \sqrt{7})/(\sqrt{13} \times \sqrt{13})$ ML domains do not promote multilayer growth but instead "seed" the dewetting process observed directly through LEEM.[35,36] Given their strong resemblance to layers of Si(111), it is also feasible that these domains are responsible for observations of HCT- or IET-like Ag segregation, which occurs on the Si(111) face.

3. Electronic Structures of Bilayers

Having explored their atomic structures, the discussion can now move on to the electronic characteristics of the freestanding and epitaxial BLs. The total and partial densities of states (DOS and pDOS, respectively) of these BLs in the vicinity of the Fermi energy are shown in **Figure 3**.

We will begin by discussing the Si pDOS of freestanding BL silicene, comparing it to that of freestanding ML silicene which we have previously reported.[13] We note a significant Si *s* and *d* contribution to the states bordering the bandgap, which suggests the lack of a *p*-dominated Dirac cone-like structure. We also report a bandgap opening of 0.22 eV. This is at odds with previous DFT treatments of freestanding BL silicene[39,41] which predicted a metallic electronic structure. We would argue that the insulating case is more likely, as the BL formation breaks the inversion symmetry of the ML (which is known to introduce a bandgap into silicene), and the BL represents an intermediate step between the small-gap ML case and the large-gap bulk Si(111) case.

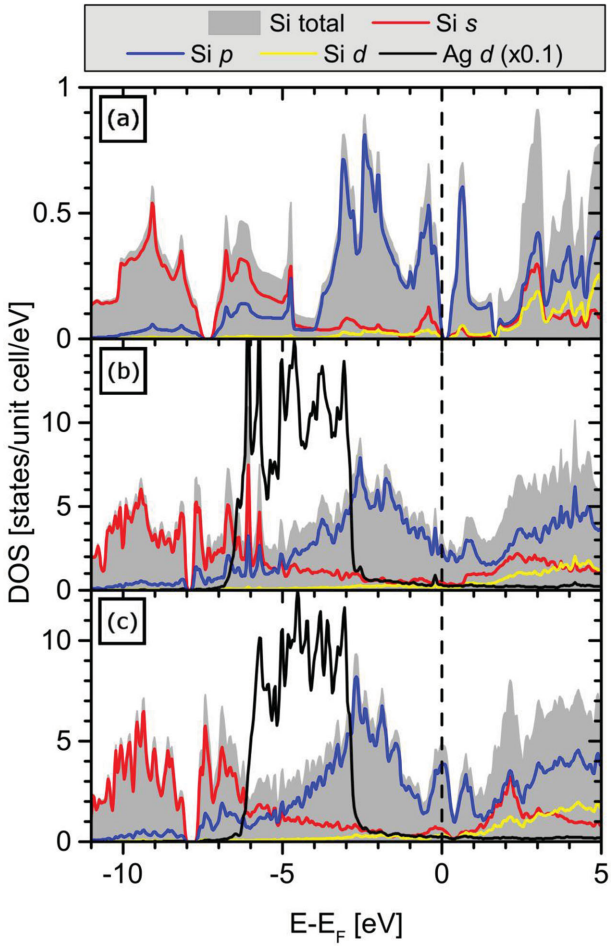

Figure 3. The Si and Ag pDOS of a) a freestanding silicene BL, b) the $(3\times3)/(4\times4)$ silicene BL, and c) the $(\sqrt{7}\times\sqrt{7})/(\sqrt{13}\times\sqrt{13})$ BL. The Fermi level is marked with a dashed line.

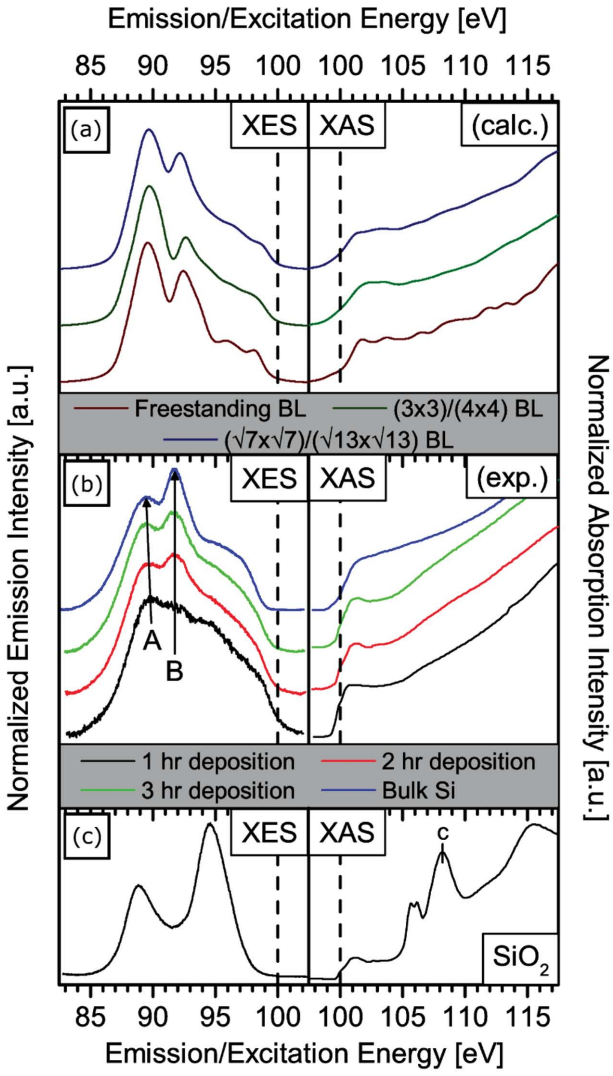

Figure 4. a) The calculated XES and XAS spectra of the silicene BLs investigated in this study. b) XES and XAS measurements of epitaxial silicene samples ranging from 1 to 3 h of deposition, as well as a bulk Si sample. c) The XES spectrum of SiO_2 and the TEY-mode XAS spectrum of the native oxide on a Si wafer, used for calibration purposes.

As for the $(3 \times 3)/(4 \times 4)$ epitaxial BL, the pDOS shows a metallic electronic structure with significant hybridization between the Ag *d* states and the Si *s* and *d* states in the region ranging from −6.5 to −3 eV, as indicated by the coincident peaks in the respective pDOS. This hybridization is less apparent than in the epitaxial $(3 \times 3)/(4 \times 4)$ ML,[13] perhaps an indication of a weakened interaction between the underlayer and substrate introduced by the presence of the overlayer. However, qualitatively the Si *s* and *d* pDOS are similar to that of the epitaxial ML, suggesting that a soft X-ray spectroscopy study of the BL should result in similar spectra.

The $(\sqrt{7} \times \sqrt{7})/(\sqrt{13} \times \sqrt{13})$ epitaxial BL also possesses a metallic electronic structure, this time with a modest peak of Si *s* and *p* states centered at E_F. Here Si *sp*–Ag *d* hybridization is far less apparent, again indicating a weakened interaction between the BL and the substrate. However, for a completely noninteracting BL on $(\sqrt{13} \times \sqrt{13})$ Ag(111) we would expect to see a pDOS similar to that of the freestanding BL given their structural similarities. We do not see this similarity, which leads us to assume that hybridization with the Ag *sp* band, located within a few eV of the Fermi level, is still significant.

We conclude that both epitaxial BLs possess similar electronic properties to their epitaxial ML counterparts. Namely, they are metallic in nature and have fairly strong hybridization with the underlying substrate. However, at least for the BL on $(\sqrt{13} \times \sqrt{13})$ Ag(111), there are some signs of weakened coupling with the substrate, which could be taken as further evidence for these structures acting as "seeds" for bulk-like crystallization.

The WIEN2k utility XSPEC, which is based on the formalism presented in ref. [42], can be used to simulate the results of XES and XAS measurements of the valence and conduction states using the calculated pDOS and experimental spectral broadening parameters. The calculated Si $L_{2,3}$ XES and 2*p* XAS for the freestanding and epitaxial BLs are presented in **Figure 4**a. The XES shows the same wedge-like profile that we have previously reported for epitaxial MLs on Ag(111), which is to be expected based on their similar *s* and *d* pDOS. Each shows three

major peaks, one at 89.5 eV, one at 92 eV, and one forming the high-energy shoulder at 98.5 eV. As was the case with the MLs, the BL XAS shows one major feature around 102 eV but is otherwise relatively featureless. Together, the simulated XES and XAS indicate that all three types of BL would be difficult to distinguish from one another, aside perhaps from the downward-shifted valence band maximum in the XES in the freestanding BL, resulting from the 0.22 eV bandgap opening.

Typically when attempting to simulate an XAS measurement, it is important to consider the effect of the core-hole (CH) introduced in the targeted atom during the process of a measurement. This CH can have significant effects on the outcome of the XAS measurement, including a downward shift in the energy of the absorption onset as well as an enhancement of the spectral features near the onset. When the XAS is plotted together with the XES these effects typically manifest themselves as a reduction in the apparent bandgap and an increased spectral weight at the bottom of the XAS.

In our case, with 28 to 36 unique Si sites per unit cell it is not feasible to simulate the effects of a CH in each site. However, we have previously shown[13] that for the metallic epitaxial MLs, which have approximately the same electronic structure as the epitaxial BLs, there is no appreciable CH shift in our XAS measurements, only an enhancement of the spectra at the bottom of the conduction band. It is reasonable to assume that the same will be true of the epitaxial BLs.

4. Sample Synthesis

We now turn to experimental characterization of epitaxial multilayers on Ag(111). Our samples for this study are produced in the typical manner of physical vapor deposition of a Si wafer on to a single-crystal disk of Ag(111) held at 500 K. Before each deposition, the Ag disk is cleaned with two consecutive cycles of Ar^+ sputtering with an Ar pressure of 10^{-6} Torr and annealing at 500 °C. The depositions take place in an ultrahigh vacuum (UHV) chamber with a base pressure of 1×10^{-9} Torr. With our source and sample geometry, we find that a complete ML forms after 1 h of deposition time, according to the absence of strong $(\sqrt{3} \times \sqrt{3})$R30° points on the LEED pattern (see Figure 1a). Our 1 h deposition parameters resulted in a mixed $(3 \times 3)/(4 \times 4)$ and $(\sqrt{7} \times \sqrt{7})/(\sqrt{13} \times \sqrt{13})$ ML, as mentioned previously.

Doubling and tripling the 1 h deposition time required to form a ML should, if large-scale multilayers of epitaxial silicene exist, roughly form a BL and a trilayer (TL), respectively. Upon depositing more Si, the LEED features associated with the $(3 \times 3)/(4 \times 4)$ and $(\sqrt{7} \times \sqrt{7})/(\sqrt{13} \times \sqrt{13})$ ML (blue and red, respectively, in Figure 1d) begin to fade and the characteristic points arising from a multilayer (green in Figure 1d) dominate the LEED pattern. Further Si deposition up to 8 h is found to simply result in the strengthening of these multilayer LEED features.

After structural characterization via LEED is complete, the samples are transferred into a high-vacuum (HV) transfer cart (base pressure 5×10^{-8} Torr) for approximately 10 to 15 min before being loaded into the soft X-ray spectroscopy measurement chamber (base pressure better than 10^{-9} Torr). The expected net exposure of the samples prior to measurement is approximately 90 L.

5. Soft X-Ray Spectroscopy

Characterization of the electronic structure of our experimental samples is achieved through soft X-ray emission and absorption spectroscopies at the Si $L_{2,3}$-edge. These processes allow us to probe the element- and orbital-specific pDOS the valence and conduction bands, respectively, by directly or indirectly monitoring transitions to and from selected core levels. In our case, we excite the Si 2*p* states, thus probing the Si *s* and *d* states in the valence and conduction bands due to the dipole transition selection rules. While it would be preferable to probe the Si *p* states that dominate the electronic structure near the Fermi level, the large incident X-ray energies required for a Si K-edge measurement (approximately 1.8 keV) render the penetration depth of the photons too large to achieve a useful signal from an atomically thin surface layer of Si atoms. Exciting at an extremely grazing incidence angle will increase the photons' path length through the silicene, but it also has the deleterious effect of increasing the beam footprint on the sample and therefore decreasing the resolving power and count rate of the XES measurement.

These soft X-ray spectroscopy measurements were performed at the XES endstation of the REIXS beamline (10-ID2) at the Canadian Light Source at the University of Saskatchewan. The monochromator resolving power ($E/\Delta E$) was 1×10^4 at the Si $L_{2,3}$-edge energy. The emission spectrometer, which uses diffraction gratings in a Rowland circle geometry as dispersive elements and is fitted with a microchannel plate detector, had a resolving power of $(E/\Delta E) = 10^3$ in the same energy region. Oxygen K-edge X-ray absorption spectra were obtained prior to Si $L_{2,3}$-edge measurements to ensure that the sample had not oxidized significantly during the in vacuo transfer from the preparation chamber to the measurement chamber. No significant O K-edge onset was observed. The elliptically polarizing undulator was tuned to produce horizontally polarized photons. All reported measurements were performed with an incidence angle of 70° from the normal, and the XES spectrometer collected photons at 90° from the incident beam. The spot size of the incident X-ray beam was approximately 20×50 μm, which is much larger than the typical continuous silicene domain on the Ag(111) surface. This indicates that our measurements should represent the qualities of the bulk silicene sample and not those of a single domain.

XAS data were calibrated such that the Si–O hybridization feature labeled "c" in Figure 4 in the total electron yield (TEY) absorption spectrum of the native surface oxide on a Si wafer occurred at 108.1 eV. A series of elastic scattering measurements was used to scale and shift the energy axis of the spectrometer to agree with that of the monochromator, providing a consistent energy calibration between the XES and XAS.

As we reported previously in the first soft X-ray spectroscopy study of ML silicene,[13] the ML XES and XAS spectra are in good agreement with the calculated spectra acquired through DFT. The BL spectra, which from our DFT simulations should resemble that of the ML, instead appear to take on features of the sp^3-hybridized bulk Si spectra (which are shown in blue in Figure 4b). A peak (labeled "B") appears at 91.5 eV in the BL XES and is more pronounced in the TL XES, coincident with the main feature in the bulk Si emission spectrum. There is

also a slight downward shift of the peak at 89.5 eV ("A") in the ML spectrum, indicating that the bulk-like states located slightly lower in energy at 89 eV are beginning to dominate the main emission feature of the ML. The top of the ML valence band, which is marked with a dashed line in Figure 4, appears to shift downward with the addition of Si. This could be taken as evidence of the formation of a BL with a bandgap opening, but it could also be the result of an increased proportion of semiconducting bulk Si to metallic epitaxial Si. The observed XAS could be said to represent a transition to the bulk Si spectrum from the ML XAS due of the emergence of the low-energy shoulder at 100 eV with additional Si layers. However, CH calculations are likely to modify the predicted XAS in this low-energy region, so it is possible that this low-energy shoulder could also be a feature of the BLs we modeled.

Together these soft X-ray spectroscopy measurements indicate that as the second and third layers of Si are deposited, bulk-like Si begins to dominate the Ag surface. Since epitaxial or freestanding BLs would not be expected to have a bulk-like emission spectrum, our result agrees with the LEEM experiment[35,36] that reported the progression from Si MLs to bulk-like crystals. However, there is still evidence of some interaction with the Ag surface, which could indicate stable epitaxial multilayer regions among the bulk-like crystals, but could also be a result of the interaction between the substrate and the crystals themselves.

6. Conclusion

To summarize, we show that DFT can be used to predict the structures of the most stable BLs on the Ag(111) (4 × 4) and ($\sqrt{13} \times \sqrt{13}$) supercells, and suggest that the (4 × 4) supercell hosts an AA-stacked structure that conforms to the ($\sqrt{3} \times \sqrt{3}$) R30° topology that has been observed using STM and non-contact atomic force microscopy. We also find that the BL on the ($\sqrt{13} \times \sqrt{13}$) supercell shows evidence of a reduced interaction with the underlying substrate. This BL, however, does not conform to any STM measurements of the Si/Ag(111) surface, which suggests that it does not exist in multilayer silicene samples. In order to explain the absence of this BL in STM data, we propose that the ($\sqrt{7} \times \sqrt{7}$)/($\sqrt{13} \times \sqrt{13}$) ML domains could act as a seed for bulk Si crystallization, or possibly Ag surface segregation.

Our electronic structure calculations indicate that both BLs should have approximately the same electronic structure as their ML counterparts, namely, metallic, strongly interacting with the substrate and without a Dirac cone at the Fermi level. This result conflicts with previous ARPES observations of a Dirac cone-like dispersion in the BL and multilayer bandstructures.[26,27] However, it is possible that these observed structures are actually metallic hybridized bands with saddle points, much like those observed in the epitaxial MLs.[8,22]

Through soft X-ray spectroscopy, we conclude that bulk-like Si is predominantly formed on the surface during the deposition of what would be a second and third layer of Si, were large-area silicene multilayers to exist. It would be interesting to determine if bulk Si formation occurred as strongly on a BL deposited on a quasi-pure phase (3×3)/(4×4) ML, which could confirm our suspicion that the ($\sqrt{7} \times \sqrt{7}$)/($\sqrt{13} \times \sqrt{13}$) ML "seeds" the dewetting process. It is also a distinct possibility that multilayer formation is even more sensitive to deposition conditions like substrate temperature and Si flux than ML formation. The difference between accounts of large-scale silicene multilayer formation and those of Ag-terminated Si or bulk Si crystallization could be the result of minute differences in growth parameters.

Acknowledgements

The authors gratefully acknowledge the contributions of Prof. Guy Le Lay, Dr. Patrick Vogt, Dr. Paola De Padova, and Dr. Andrea Resta for their invaluable experimental guidance. The authors would also like to acknowledge financial support from the Natural Sciences and Engineering Research Council of Canada (NSERC), the Canada Research Chair Program, and the Russian Foundation for Basic Research (Projects 14-02-00006). Calculations utilized Compute Canada's WestGrid HPC consortium. Research was performed at the REIXS beamline of the Canadian Light Source, which was supported by NSERC, the National Research Council (Canada), the Canadian Institutes of Health Research, the Province of Saskatchewan, Western Economic Diversification Canada, and the University of Saskatchewan.

Received: March 16, 2015
Revised: April 23, 2015
Published online: May 22, 2015

[1] A. K. Geim, K. S. Novoselov, *Nat. Mater.* **2007**, *6*, 183.
[2] Q. Tang, Z. Zhou, *Prog. Mater. Sci.* **2013**, *58*, 1244.
[3] S. Cahangirov, M. Topsakal, E. Aktürk, H. Sahin, S. Ciraci, *Phys. Rev. Lett.* **2009**, *102*, 236804.
[4] A. Kara, H. Enriquez, A. P. Seitsonen, L. Lew Yan Voon, S. Vizzini, B. Aufray, H. Oughaddou, *Surf. Sci. Reports* **2012**, *67*, 1.
[5] C.-C. Liu, W. Feng, Y. Yao, *Phys. Rev. Lett.* **2011**, *107*, 076802.
[6] Z. Ni, Q. Liu, K. Tang, J. Zheng, J. Zhou, R. Qin, Z. Gao, D. Yu, J. Lu, *Nano Lett.* **2012**, *12*, 113.
[7] W.-F. Tsai, C.-Y. Huang, T.-R. Chang, H. Lin, H.-T. Jeng, A. Bansil, *Nat. Commun.* **2013**, *4*, 1500.
[8] P. Vogt, P. De Padova, C. Quaresima, J. Avila, E. Frantzeskakis, M. Asensio, A. Resta, B. Ealet, G. Le Lay, *Phys. Rev. Lett.* **2012**, *108*, 155501.
[9] H. Jamgotchian, Y. Colignon, N. Hamzaoui, B. Ealet, J. Y. Hoarau, B. Aufray, J. P. Bibérian, *J. Phys.: Condens. Matter* **2012**, *24*, 172001.
[10] J. Gao, J. Zhao, *Sci. Rep.* **2012**, *2*, 861.
[11] H. Enriquez, S. Vizzini, A. Kara, B. Lalmi, H. Oughaddou, *J. Phys.: Condens. Matter* **2012**, *24*, 314211.
[12] E. Cinquanta, E. Scalise, D. Chiappe, C. Grazianetti, B. V. D. Broek, M. Houssa, M. Fanciulli, A. Molle, *J. Phys. Chem. C* **2013**, *117*, 16719.
[13] N. W. Johnson, P. Vogt, A. Resta, P. De Padova, I. Perez, D. Muir, E. Z. Kurmaev, G. Le Lay, A. Moewes, *Adv. Funct. Mater.* **2014**, *24*, 5253.
[14] L. Meng, Y. Wang, L. Zhang, S. Du, R. Wu, L. Li, Y. Zhang, G. Li, H. Zhou, W. A. Hofer, H.-J. Gao, *Nano Lett.* **2013**, *13*, 685.
[15] D. Chiappe, E. Scalise, E. Cinquanta, C. Grazianetti, B. van den Broek, M. Fanciulli, M. Houssa, A. Molle, *Adv. Mater.* **2014**, *26*, 2096.
[16] A. Fleurence, R. Friedlein, T. Ozaki, H. Kawai, Y. Wang, Y. Yamada-Takamura, *Phys. Rev. Lett.* **2012**, *108*, 1.
[17] H. Liu, J. Gao, J. Zhao, *J. Phys. Chem. C* **2013**, *117*, 10353.

[18] T. P. Kaloni, M. Tahir, U. Schwingenschlögl, *Sci. Rep.* **2013**, *3*, 3192.
[19] A. Resta, T. Leoni, C. Barth, A. Ranguis, C. Becker, T. Bruhn, P. Vogt, G. Le Lay, *Sci. Rep.* **2013**, *3*, 2399.
[20] Z.-L. Liu, M.-X. Wang, C. Liu, J.-F. Jia, P. Vogt, C. Quaresima, C. Ottaviani, B. Olivieri, P. Padova De, G. Le Lay, *APL Mater.* **2014**, *2*, 035448.
[21] Y.-P. Wang, H.-P. Cheng, *Phys. Rev. B* **2013**, *87*, 245430.
[22] D. Tsoutsou, E. Xenogiannopoulou, E. Golias, P. Tsipas, A. Dimoulas, *Appl. Phys. Lett.* **2013**, *103*, 231604.
[23] R. Stephan, M.-C. Hanf, P. Sonnet, *J. Phys.: Condens. Matter* **2015**, *27*, 015002.
[24] C.-L. Lin, R. Arafune, K. Kawahara, M. Kanno, N. Tsukahara, E. Minamitani, Y. Kim, M. Kawai, N. Takagi, *Phys. Rev. Lett.* **2013**, *110*, 076801.
[25] L. Tao, E. Cinquanta, D. Chiappe, C. Grazianetti, M. Fanciulli, M. Dubey, A. Molle, D. Akinwande, *Nat. Nanotechnol.* **2015**, *10*, 227.
[26] P. De Padova, J. Avila, A. Resta, I. Razado-Colambo, C. Quaresima, C. Ottaviani, B. Olivieri, T. Bruhn, P. Vogt, M. C. Asensio, G. Le Lay, *J. Phys.: Condens. Matter* **2013**, *25*, 382202.
[27] P. De Padova, P. Vogt, A. Resta, J. Avila, I. Razado-Colambo, C. Quaresima, C. Ottaviani, B. Olivieri, T. Bruhn, T. Hirahara, T. Shirai, S. Hasegawa, M. Carmen Asensio, G. Le Lay, *Appl. Phys. Lett.* **2013**, *102*, 163106.
[28] P. Vogt, P. Capiod, M. Berthe, A. Resta, P. De Padova, T. Bruhn, G. Le Lay, B. Grandidier, *Appl. Phys. Lett.* **2014**, *104*, 021602.
[29] A. J. Mannix, B. Kiraly, B. L. Fisher, M. C. Hersam, N. P. Guisinger, *ACS Nano* **2014**, *8*, 7538.
[30] T. Shirai, T. Shirasawa, T. Hirahara, N. Fukui, T. Takahashi, S. Hasegawa, *Phys. Rev. B* **2014**, *89*, 241403.
[31] P. De Padova, C. Ottaviani, C. Quaresima, B. Olivieri, E. Imperatori Salomon, T. Angot, L. Quagliano, C. Romano, A. Vona, M. Muniz-Miranda, A. Generosi, B. Paci, G. Le Lay, *2D Mater.* **2014**, *1*, 021003.
[32] D. Kaltsas, L. Tsetseris, *Phys. Chem.: Chem. Phys.* **2013**, *15*, 9710.
[33] S. Cahangirov, M. Audiffred, P. Tang, A. Iacomino, W. Duan, G. Merino, A. Rubio, *Phys. Rev. B* **2013**, *88*, 035432.
[34] Z.-X. Guo, A. Oshiyama, *Phys. Rev. B* **2014**, *89*, 155418.
[35] A. Acun, B. Poelsema, H. J. W. Zandvliet, R. van Gastel, *Appl. Phys. Lett.* **2013**, *103*, 263119.
[36] P. Moras, T. O. Mentes, P. M. Sheverdyaeva, A. Locatelli, C. Carbone, *J. Phys.: Condens. Matter* **2014**, *26*, 185001.
[37] K. Schwarz, P. Blaha, G. Madsen, D. Kvasnicka, J. Luitz, *Wien2k. An Augmented Plane Wave + Local Orbitals Program for Calculating Crystal Properties*, Universität Wien, Austria **2001**.
[38] J. Perdew, K. Burke, M. Ernzerhof, *Phys. Rev. Lett.* **1996**, *77*, 3865.
[39] B. Mohan, A. Kumar, P. Ahluwalia, *Phys. E* **2013**, *53*, 233.
[40] J. Tersoff, D. Hamann, *Phys. Rev. B* **1985**, *31*, 805.
[41] C. Kamal, A. Chakrabarti, A. Banerjee, S. K. Deb, *J. Phys.: Condens. Matter* **2013**, *25*, 085508.
[42] K. Schwarz, A. Neckel, J. Nordgren, *J. Phys. F: Met. Phys.* **1979**, *9*, 2509.
[43] K. Momma, F. Izumi, *J. Appl. Crystallogr.* **2011**, *44*, 1272.